Isolating an origin of Rashba spin splitting within inverted doped sGe heterostructures.

A.H.A. Hassan[1], R.J.H. Morris[2, 3], O.A. Mironov[3], S. Gabani, A. Dobbie[3], M. Myronov[3], and D.R. Leadley[3]

[1] Department of Physics, University of Tripoli, Tripoli, Libya.

[2] Current address: IMEC, Kapeldreef 75, B-3001 Leuven, Belgium

[3] Department of Physics, University of Warwick Coventry, CV4 7AL, UK,

Abstract

In this paper we demonstrate an origin for cubic Rashba spin splitting observed within inverted doped strained germanium (sGe) hetrostructures. Magnetotransport measurements showed beating within the SdH data, with ensuing Fast Fourier analysis revealing cubic Rashba spin splitting to be present. A spin orbit interaction value of $\beta = 0.7 \times 10^{-28}$ eVm^3 and spin-splitting energy $\Delta = 0.9$ meV were determined. The source of the cubic Rashba spin splitting was identified from a combination of ultra low energy secondary ion mass spectrometry analysis and subsequent band structure modelling using Nextnao[3]. Ultra low energy secondary ion mass spectrometry revealed an unintentional, highly B doped near surface region to be present. By incorporating this information into the Nextnano[3] modelling, two single subband triangular QWs were predicted, one at the upper and the other at the lower interface of the sGe QW. Moreover, these triangular wells are expected to be asymmetric due to the difference in B doping levels and spacer layer thicknesses, and it is this asymmetry which induces the cubic Rashba spin splitting observed.

There is a growing interest in spin based devices which has led to a significant interest in the phenomena of the spin orbit interaction[1]. Advantages of a spintronic device compared to the current electronic type are lower power consumption and higher data processing speeds[1]. One particular device that would significantly benefit is the spin field effect transistor (FET) which utilizes the Rashba spin precession. This can be controlled by manipulation of the spin orbit coupling in a way analogous to that of a gate voltage in a typical FET[2-4]. Given the dominance of Si within the microelectronics industry, producing a Si spin transistor or a spin transistor from another material which offers enhanced performance parameters but is easily integrated with Si e.g. Ge, would be of significant interest. To achieve zero spin splitting, either bulk inversion asymmetry or structural inversion asymmetry[5] must be realized. However, bulk Si and Ge have a diamond structure which exhibits a high level of symmetry and so to achieve the Rashba SOI, a two dimensional heterostructure which has some means to break the symmetry needs to be adopted. Potential ways for achieving the latter is through asymmetric doping i.e. different doping concentration either side of the highly conducting channel, or manipulating the electric field within the sample using a gate voltage. Moreover, compressive strain in a 2D hole gas heterostruture splits the heavy and light hole valence band energy levels, thus raising the heavy hole (HH) above that of the light Hole (LH) and so making it the dominant hole transport level. For this reason, cubic Rashba SOI is believed to be the mechanism responsible for the zero magnetic field spin splitting observed in this type of material[5-8]. Previous studies have reported a weak Rashba spin splitting interaction (α) for a two dimensional electron gas in a strained Si (sSi)[9, 10] quantum well (QW) with $\alpha = 0.55\times10^{-12}$ eVm , while for a 2D hole gas in Si and/or Ge, cubic Rashba SOI (β) has been shown with values ranging between $\beta = 0.2-1\times10^{-28}$ eVm^3 [5, 7, 11, 12]

In this paper we report on two strained Ge (sGe) QW samples (11-284 and 11-285). Both samples were grown using an ASM Epsilon 2000 RP-CVD reactor with the full structure

consisting of a 100 mm diameter Si (001) substrate (10-20 Ohm-cm) on top of which was deposited a 2.1 µm thick $Si_{0.2}Ge_{0.8}$ reverse-graded buffer layer.[13] This strain tuning buffer[14] is grown without any chemical mechanical polishing (CMP) and previously found to have a low threading dislocation density (TDD) of $\leq 4\times10^6$ cm^{-2}.[13, 15] On top of the buffer a B-doped supply layer (12 ± 3 nm (11-285) and 21±3 nm (11-284)), $Si_{0.2}Ge_{0.8}$ spacer layer (23 ± 2nm (11-285) and 20 ± 2 nm (11-284)), a sGe QW (15 nm for 11-285 and 20 nm for 11-284), a further $Si_{0.2}Ge_{0.8}$ layer (38 ± 2 nm) and finally a thin (~2nm) Si cap were grown. Furthermore, the sGe QW for both samples was determined to be 0.65 ± 0.01% i.e. fully strained, using high resolution X-ray diffraction reciprocal space mapping.

For this work magnetotransport measurements were performed using a standard Hall Bar geometry (50 × 500 µm) with Al contacts deposited by thermal evaporation. From these electrical measurements [12, 16, 17] the Hall mobility of 11-285 was found to be 2.65×10^5 cm^2/Vs (sheet density $p_s = 5.2\times10^{11}$ cm^{-2}) at 20 K while an effective mass of (0.063±0.003) m_0 and Dingle ratio of 33 were determined from the Shubnikov de Hass (SdH) oscillations within the temperature range 300 mK – 900 mK[12]. For sample 11-284, a mobility of 5.09×10^5 cm^2/Vs ($p_s = 5.14\times10^{11}$ cm^{-2}) at 0.1 K was found and an effective mass of (0.070±0.002) m_0 and a Dingle ratio of 33 determined from SdH[12, 16]

In the case of sample 11-284 and for the temperature range 90 mK - 1.5 K, ρ_{xx} and ρ_{xy} were determined (Figure 1). The findings show positive magnetotransport behaviour about -0.5 T < B < 0.5 T indicating two carrier types are present with both contributing to the overall transport in this sample. These two carriers are expected to account for the beating observed in the measured signal between 1 and 3 T[18, 19]. However, the origin of this beating may arise from more than one effect and include: more than one subband occupancy, zero spin splitting, a two pocket effect caused by asymmetry in the structure or some combination of all these[20]. To try to identify the cause of the beating we performed a Fast Fourier analysis on the data

between 0.3 T and 0.9 T (see figure 2). The reason for using this limited range of the measured data was because the complicated beating in the SdH oscillations meant it was not possible to obtain any sensible or meaningful information beyond > 0.9 T. The Fast Fourier analysis revealed a single peak at f = 10.11 Hz which supports single subband occupancy while a sheet density $p_s = 4.89\times10^{11}$ cm^{-2} was also determined. A further, harmonic, peak is observed at double the frequency (f = 20.22 Hz) which results from the non-sinusoidal oscillations. The calculated p_s value from the Fast Fourier analysis is found to be slightly lower (~5%) than that determined from the slope of the Hall resistance where the calculation of p_s depends upon the selected interval of magnetic field. The single carrier peak found from the Fast Fourier analysis negates zero field spin splitting in this structure. Thus it must be concluded that the beating combined with the positive magnetotransport behaviour observed (i.e. two carrier transports) must be from a second conduction channel (i.e. second pocket) with a different carrier mobility. To explore this multiple channel carrier mobility further, self-consistent Poisson-Schrödinger modelling of the intended sample band structure using Nextnano[3] was performed (figure 3). From figure 3 it is seen that a single triangular QW at the sGe QW interface closest to the doping layer (dotted line figure 3) is predicted and with only one subband being occupied i.e. above the Fermi energy E_f. This was in contrast to the results obtained. However, from the ultra-low energy secondary ion mass spectrometry (uleSIMS) analysis of 11-284 (figure 4), a very thin layer of high concentration B is observed at the region near the sample surface. By including this unintentional doping into our Nextnano[3] model it leads to the prediction of a second triangular well, this time at the sGe interface closest to the sample surface (figure 3). Again the simulation shows only one subband is occupied in this second QW while the two triangular wells either side of the sGe QW are (almost) pinched off in the middle. Hence, we appear to have the beginning of two separate conducting channels (two pocket) and a potential reason for the two type of carriers measured. The predicted band

asymmetry of the two triangular QW pockets, as observed from figure 3, will result in an asymmetric electric field on the carriers, potential differences in HH energy levels if pinch off occurs, while the quality of each interface will necessarily be different and lead to variation in the interface roughness scattering, any of which could lead to the complicated beating observed in the magnetotransport data and inhibit spin splitting.

Magnetotransport measurements from an identical Hall bar sample but this time sample 11-285 are shown in (figure 5) for the temperature range 300 mK to 15 K and magnetic field -2T < B < 2 T. The SdH oscillations for the lowest temperature appear at ± 0.4 T, with the SdH beating occurring over different temperatures and up to 1 K (not shown). The magnetotransport behaviour observed for 11-285 between -0.5 T < B < 0.5 T is different to 11-284 in that this time we have negative magnetotransport behaviour which is indicative of only a single carrier being present, behaviour previously seen where spin splitting in GaAs [21] was found. By increasing the temperature to ≥ 1.5 K the beating disappeared. Fast Fourier analysis was again performed (insert of Figure 5), this time on the 300 mK data and for magnetic fields between $0.3 \leq B \leq 2$ T. The Fast Fourier analysis shows two peaks at almost the same frequency (f_1 = 12.2 Hz and f_2 = 13.2 Hz), indicating two sets of hole densities within two spin-split states. The sheet density of the up and down Rashba spin splitting states were calculated to be $p_1 = 2.95 \times 10^{11}$ cm^{-2} and $p_2 = 3.19 \times 10^{11}$ cm^{-2}. A third peak at f_3 = 25.3 Hz with a corresponding sheet density of $p_t = 6.02 \times 10^{11}$ cm^{-2} is also seen[21]. Finally, a small peak f_4 = 38 Hz is observed which corresponds to $f_1 + f_3$ and is believed to be from Zeeman spin splitting[5, 11]. Spin splitting of the HH level has been shown to occur because of cubic Rashba SOI[7], while for the LH linear Rashba SOI. Given that our sample is under compressive strain, hence, the dominant conduction channel is the HH level, the cubic Rashba coefficient was calculated using the following equation[5, 7]

$$\beta = \sqrt{\frac{2}{\pi}} \frac{\hbar^2}{2m^*} \frac{p(p_+ - p_-) + \Delta p(p_+ + p_-)}{6p^2 + 2\Delta p^2} \quad (1)$$

Where m* is the hole effective mass calculated from the SdH amplitude as function of temperature[22] (m* = 0.063±0.003×m_0 for sample 11-285) and $p_\pm = \sqrt{p \pm \Delta p}$, where p is the sum between spin up and spin down sheet densities and Δp their difference. From our analysis we determine β to be 0.7×10^{-28} eVm^3 which is in good agreement with values previously found. A spin-splitting energy (Δ) of 0.9 meV was also found by using $\Delta = 2\beta k^3$ where the Fermi wavevector (k) is taken to be $k = 1.8\times10^8$ m.

By incorporating the high level of near surface B doping found by uleSIMS into our Nextnano[3] simulation, we are able to explain where the beating observed in the magnetotransport data for sample 11-284 arises from. The uleSIMS for 11-285 (not shown) also showed a similarly high B concentration within the Si cap and so adopting the same approach we modelled the band structure of 11-285. Figure 6 shows the Nextnano[3] simulation for 11-285 and once again we find two pockets of carriers in the sGe QW are predicted. However, as this sample has a much thinner QW, the single occupied subband for each pocket is not close to being pinched off at the centre of the QW, as was the case of 11-284. Thus, the zero spin splitting observed is believed to arise from the asymmetry present in the Sge QW band structure caused by the significant difference in doping levels either side of the sGe QW necessitating the carriers to experience an asymmetric field.

By reducing the sGe QW thickness further but keeping all the other parameters constant, we expect an enhancement in the zero spin splitting to occur while increasing the sGe QW thickness would only result in strengthening the case for two isolated QWs at each interface. More importantly, our findings indicate and reaffirm that a sGe heterostructure does offer the potential for spintronic devices with the significant advantage of being compatible with current Si technology.

In conclusion, we have measured the magnetotransport of two inverted B doped high mobility sGe 2DHG samples. From the beating behavior found in the SdH data, Fast Fourier analysis was performed with cubic Rashba spin splitting observed. The origin of the cubic Rashba spin splitting within the inverted sGe heterostrutures was identified using a combination of uleSIMS analysis and subsequent Nextnao[3] modelling. Due to an unintentional high B doping spike found at the sample surface, and its incorporation into the Nextnao[3] modelling, revealed a significantly modified band structure whereby a second triangular QW is formed at the opposite QW interface. This results in breaking the Ge structure symmetry and enabling spin splitting to occur. Fast Fourier analysis of the thinner (15 nm) sGe QW revealed weak Rashba spin splitting with a spin orbit interaction value of $\beta = 0.7 \times 10^{-28}$ eVm^3 and a spin-splitting energy of $\Delta = 0.9$ meV.

Acknowledgements

AHAH would like to thank C. Morrison for his help in preparing the Hall bars measured for this work.

Samples	T K	ρ_{xx} Ohm/sq	p_{sHall} $\times 10^{11}$cm^{-2}	p_{sFFA} $\times 10^{11}$ cm^{-2}	μ $\times 10^{5}$ cm^2/Vs	l_m μm	τ_t ps	k_F $\times 10^{8}$ m^{-2}
11-285	0.3	23.17	6.02	6.02	4.48	5.73	16.0	1.94
11-284	0.1	23.87	5.14	4.89	5.09	6.03	20.3	1.79

Table 1. Hole transport parameters for samples 11-285 and 11-284.

1. S. A. Wolf, D. D. Awschalom, R. A. Buhrman, J. M. Daughton, S. von Molnár, M. L. Roukes, A. Y. Chtchelkanova and D. M. Treger, Science **294** (5546), 1488-1495 (2001).
2. G. Engels, J. Lange, T. Schäpers and H. Lüth, Physical Review B **55** (4), R1958-R1961 (1997).
3. J. M. Lagemaat, G. E. W. Bauer, J. J. Harris and C. T. Foxon, Physical Review B **38** (18), 13439-13442 (1988).
4. S. N. Holmes, P. J. Simmonds, H. E. Beere, F. Sfigakis, I. Farrer, D. A. Ritchie and M. Pepper, Journal of Physics: Condensed Matter **20** (47), 472207 (2008).
5. R. Winkler, Springer Tracts in Modern Physics, (Springer, Berlin, 2003), Vol. 191 (2003).
6. G. M. Minkov, A. A. Sherstobitov, A. V. Germanenko, O. E. Rut, V. A. Larionova and B. N. Zvonkov, Physical Review B **71** (16), 165312 (2005).
7. R. Moriya, K. Sawano, Y. Hoshi, S. Masubuchi, Y. Shiraki, A. Wild, C. Neumann, G. Abstreiter, D. Bougeard, T. Koga and T. Machida, Physical Review Letters **113** (8), 086601 (2014).
8. H. Nakamura, T. Koga and T. Kimura, Physical Review Letters **108** (20), 206601 (2012).
9. Z. Wilamowski, W. Jantsch, H. Malissa and U. Rössler, Physical Review B **66** (19), 195315 (2002).
10. Z. Wilamowski, W. Jantsch, N. Sandersfeld, M. Mühlberger, F. Schäffler and S. Lyon, Physica E: Low-dimensional Systems and Nanostructures **16** (1), 111-120 (2003).
11. C. Morrison, P. Wiśniewski, S. D. Rhead, J. Foronda, D. R. Leadley and M. Myronov, Applied Physics Letters **105** (18), 182401 (2014).
12. A.H.A. Hassan, PhD Thesis, University of Warwick (2014).
13. V. A. Shah, A. Dobbie, M. Myronov, D. J. F. Fulgoni, L. J. Nash and D. R. Leadley, Applied Physics Letters **93** (19) (2008).
14. M. Myronov, A. Dobbie, V. A. Shah, X. C. Liu, V. H. Nguyen and D. R. Leadley, Electrochemical and Solid State Letters **13** (11), H388-H390 (2010).
15. V. A. Shah, A. Dobbie, M. Myronov and D. R. Leadley, Journal of Applied Physics **107** (6) (2010).
16. A. H. A. Hassan, O. A. Mironov, A. Dobbie, J. H. Morris, J. E. Halpin, V. A. Shah, M. Myronov, D. R. Leadley, S. Gabani, A. Feher, E. Cizmar, V. V. Andrievskii and I. B. Berkutov, presented at the Electronics and Nanotechnology (ELNANO), 2013 IEEE XXXIII International Scientific Conference, 2013 (unpublished).
17. A. H. A. Hassan, R. J. H. Morris, O. A. Mironov, R. Beanland, D. Walker, S. Huband, A. Dobbie, M. Myronov and D. R. Leadley, Applied Physics Letters **104** (13), 132108 (2014).
18. A. M. Gilbertson, W. R. Branford, M. Fearn, L. Buckle, P. D. Buckle, T. Ashley and L. F. Cohen, Physical Review B **79** (23), 235333 (2009).
19. G. M. Minkov, A. V. Germanenko, O. E. Rut, A. A. Sherstobitov, S. A. Dvoretski and N. N. Mikhailov, Physical Review B **88** (15), 155306 (2013).
20. G. Ottaviani, C. Canali, F. Nava and J. W. Mayer, J. Appl. Phys. **44** (6), 2917-2918 (1973).
21. C. Gerl, S. Schmult, H.-P. Tranitz, C. Mitzkus and W. Wegscheider, Applied Physics Letters **86** (25), - (2005).
22. V. V. A. Y. F. Komnik, I. B. Berkutov, S. S. Kryachko, M.Myronov, and T. E. Whall, Low Temp. Phys. **26** (8) (2000).

Figure 1 Magnetotransport measurement of sample 11-284 (11-284HB4b) showing ρ_{xx} and ρ_{xy} at over the temperature range 90 mK–1.5 K.

Figure 2. Fast Fourier analysis of the magnetoresistance data taken at 90 mK from sample 11-284 (11-284-HB6) for a magnetic field of 0.3 T < B < 0.9 T.

Figure 3. Nextnano^3 simulation of sample 11-284 using the 6 × 6 k.p. method and applying the B doping values measured using uleSIMS for both the intentional doping layer and the unintentionally doped Si cap.

Figure 4. uleSIMS depth profile showing the Si, Ge and B concentration as a function of depth for the inverted structure 11-284.

Figure 1. ρ_{xx} as a function of magnetic field for sample 11-285 (Insert shows the Fast Fourier analysis of the 300 mK data).

Figure 2. Nextnano^3 simulation of sample 11-284 using the 6 × 6 k.p method and applying the B doping values measured using uleSIMS for both the intentional doping layer and the unintentionally doped Si cap.

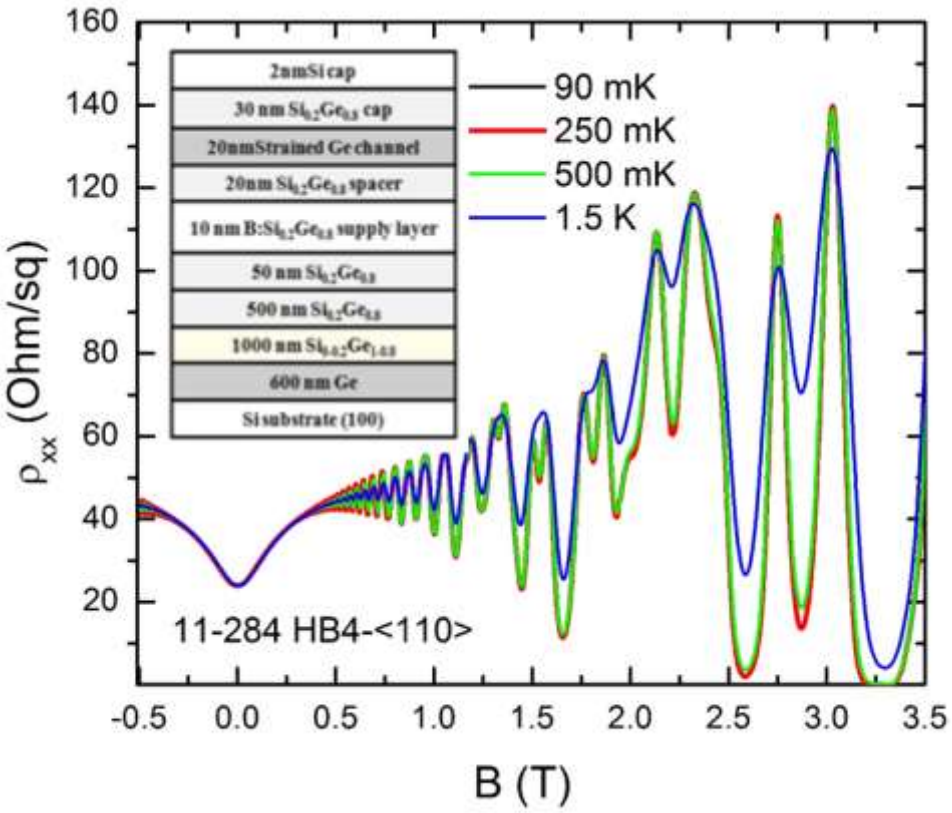

Figure 1 Magnetotransport measurement of sample 11-284 (11-284HB4b) showing ρ_{xx} and ρ_{xy} at over the temperature range 90 mK–1.5 K.

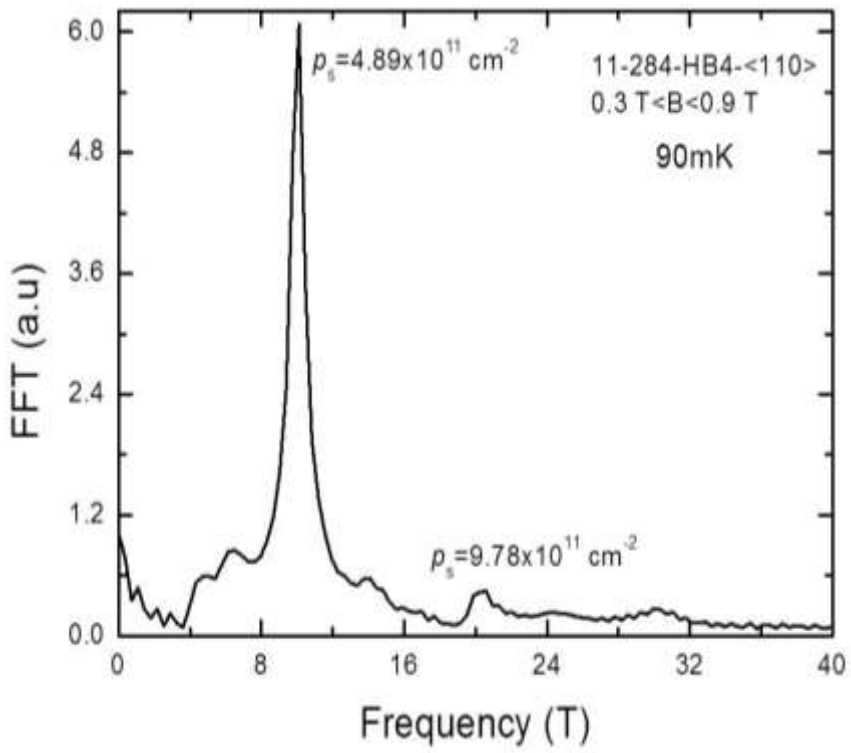

Figure 2. Fast Fourier analysis of the magnetoresistance data taken at 90 mK from sample 11-284 (11-284-HB6) for a magnetic field of 0.3 T < B < 0.9 T.

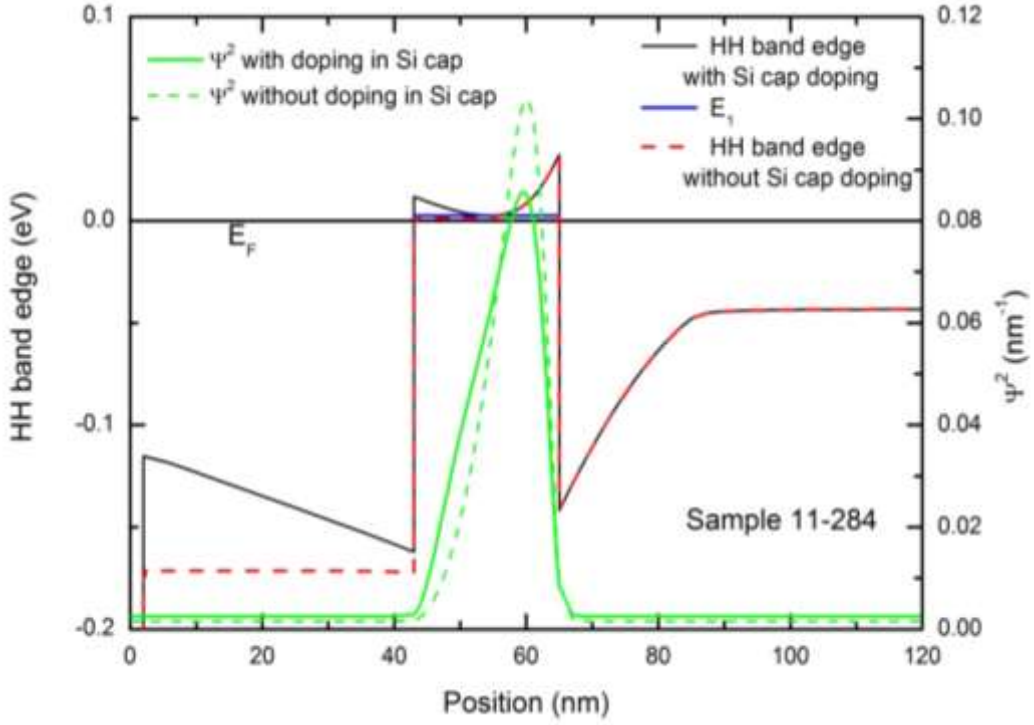

Figure 3. Nextnano[3] simulation of sample 11-284 using the 6 × 6 k.p. method and applying the B doping values measured using uleSIMS for both the intentional doping layer and the unintentionally doped Si cap.

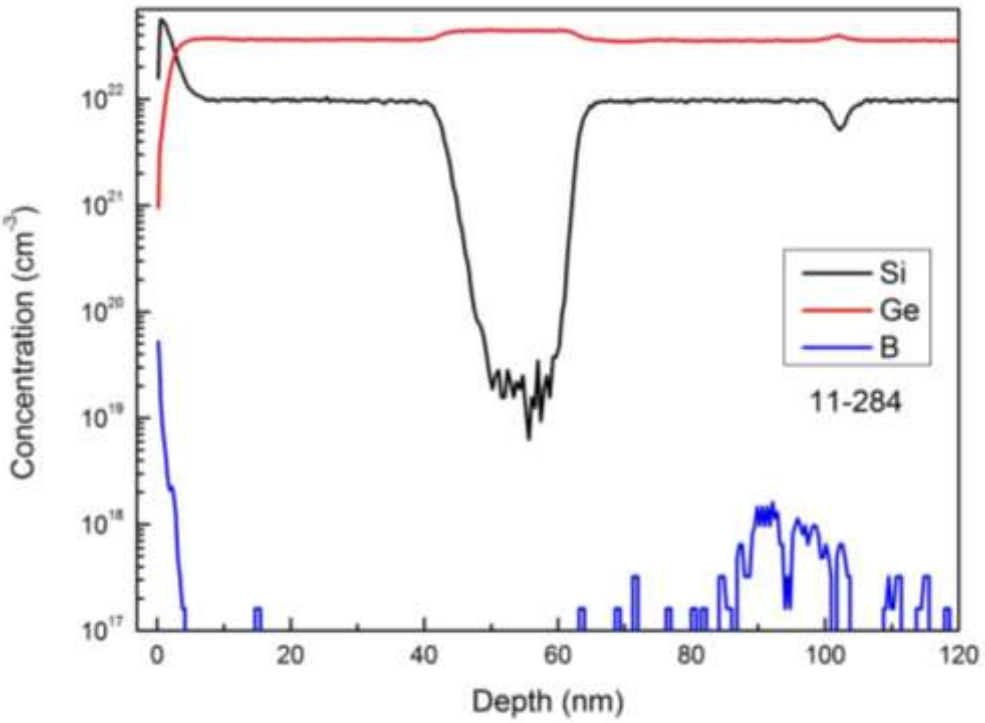

Figure 4. uleSIMS depth profile showing the Si, Ge and B concentration as a function of depth for the inverted structure 11-284.

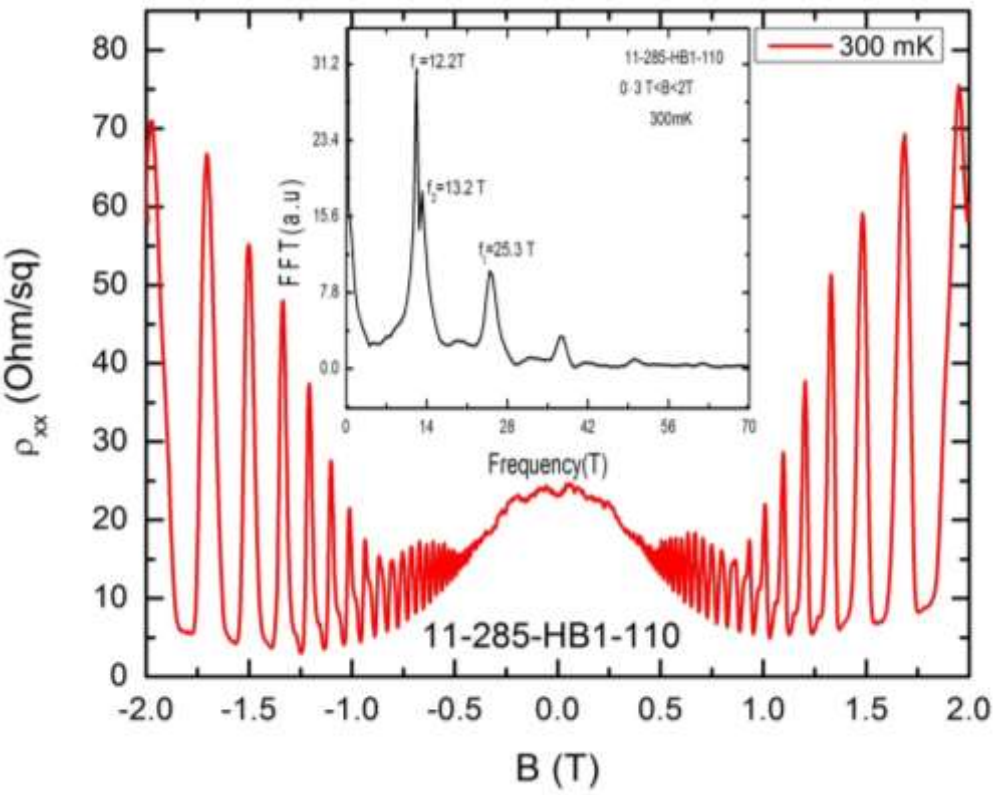

Figure 3. ρ_{xx} as a function of magnetic field for sample 11-285 (Insert shows the Fast Fourier analysis of the 300 mK data).

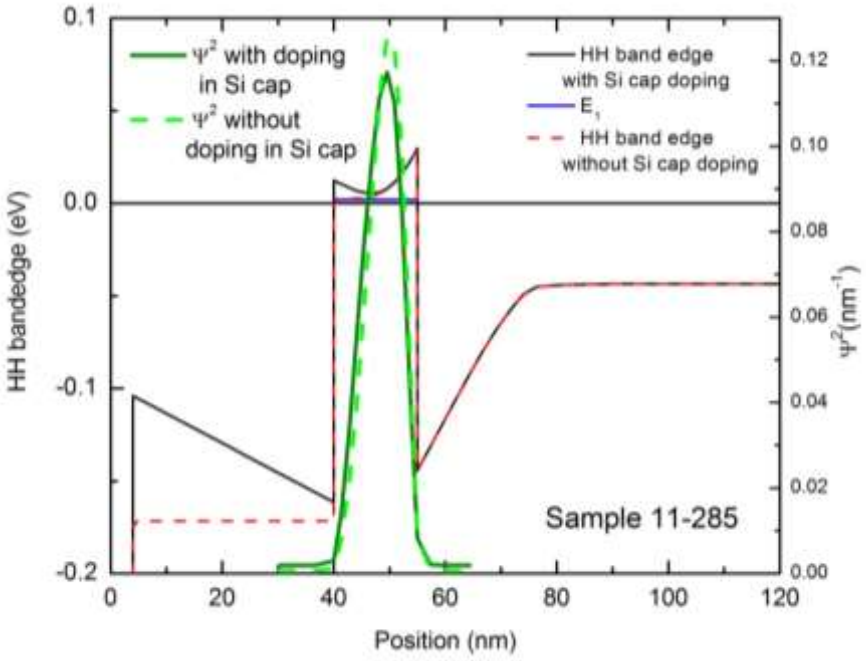

Figure 4. Nextnano[3] simulation of sample 11-284 using the 6 × 6 k.p method and applying the B doping values measured using uleSIMS for both the intentional doping layer and the unintentionally doped Si cap.